Journal Name

ARTICLE TYPE

Cite this: DOI: 00.0000/xxxxxxxxxx

Supplementary information: Perspective on the scintillating response of CdSe based nanoplatelets heterostructures

Zhu Meng,[a] Benoit Mahler,*[a] Julien Houel,[a] Florian Kulzer,[a] Andrey Vasil'ev[b], and Christophe Dujardin *[a]

Received Date
Accepted Date

DOI: 00.0000/xxxxxxxxxx

1 TEM images of the CdSe core

The 4ML CdSe nanoplatelets TEM images are presented in figure 1. They show a non rectangular shape with lateral dimensions between 10 and 20 nm.

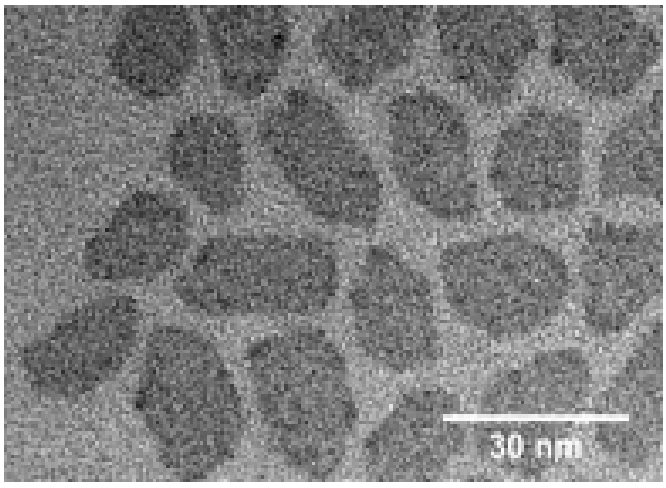

Figure 1 TEM images of the CdSe core nanoplatelets

2 Maximum-Likelihood Analysis of Multi-Exponential Decay Curves

This section provides a short summary of maximum-likelihood analysis of multi-exponential luminescence decay curves for the convenience of readers not familiar with this technique; further details can be found in a previous publication? and the references cites therein. Figures 2, 3, 4 and 5 show the first 500 nanoseconds of the photoluminescence decays of our core/shell and core/crown nanoplatelets; these data were already presented in Fig. 2 c of the main article and are now combined with the maximum-likelihood fits of models comprising one, two, three, and four exponential decay components, respectively, on a constant background. All models include convolution with the measured instrumental response function, hence the small amount of noise that is visible in the low-intensity parts of some model curves.

The agreement between data and model can be appreciated in the bottom panels of the plots, which show the normalized residuals of each channel, i. e., the difference between data and model after normalization to the square root of the model. If a given model fully describes the data, then the remaining differences are exclusively due to photon-counting noise, which is to say that the data in each channel should exhibit a Poissonian distribution around a mean value that is identical to the model prediction for the respective point in time. As the standard deviation of a Poissonian distribution is given by the square root of its average value, calculated as $(\text{data} - \text{model})/\sqrt{\text{model}}$ should then be randomly distributed around a mean value of $\mu = 0$ with a standard deviation of $\sigma = 1$. A larger standard deviation of the normalized residuals, as well as pro-

[a]*Institut Lumière Matière, UMR5306 Université Lyon 1-CNRS, Université de Lyon, 69622 Villeurbanne cedex, France; E-mail: christophe.dujardin@univ-lyon1.fr; benoit.mahler@univ-lyon1.fr*
[b]*Skobeltsyn Institute of Nuclear Physics, Lomonosov Moscow State University, 119991 Moscow, Russia.*

† Electronic Supplementary Information (ESI) available: [details of any supplementary information available should be included here]. See DOI: 00.0000/00000000.

nounced systematic deviations from the $\mu = 0$ baseline during certain periods indicate that the models with less than four exponential components do not describe the decay curves in Figs. 2 – 5 very well.

A quantitative statistical measure for the agreement between data and a given model in the presence of show noise is the Poisson deviance D, listed in the insets of Figs. 2 – 5; lower values of D indicate better agreement with the data. The reduction in D due to an additional exponential component can be used in a likelihood-ratio test to calculate the probability that such an improvement is caused purely by chance, i. e., by the fact that a greater number of free parameters leads to better adjustment to the noise in a given data curve. As each exponential components contributes two free parameters to the model (decay rate and relative contribution to the overall signal), the apparent improvement of a fit by a spurious additional component is expected to follow a χ^2-distribution with two degrees of freedom[?] . To provide an idea of orders of magnitude, a reduction of the Poisson deviance D by 70 has a probability of $p \approx 10^{-15}$ to occur by random chance; as can bee seen in Figs. 2 – 5, we achieve significantly larger reductions of D with each added exponential component and can therefore accept the four-component model for all these decay curves with a high degree of confidence, $p < 10^{-15}$.

3 Log distributed decay time fitting approach

In order to avoid a pre-defined number of exponent components, this fitting method considers a distribution of amplitudes over a pre-defined set of characteristic times. In this case the fitting function $f(t)$ is represented as the convolution of IRF (instrument response function) $i(t)$ with a sum of exponential functions:

$$f(t) = \int dt_1 i(t-t_1) \sum_i \frac{A_i}{\tau_i(1-e^{-T/\tau_i})} \times$$

$$(e^{-t_1/\tau_i}\theta(t_1) + e^{-(T+t_1)/\tau_i}\theta(T+t_1)\theta(-t_1)) \qquad (1)$$

where $A_i > 0$ are unknown coefficients, T is pulse repetition period (1 μs), and τ_i is $i-$th characteristic time from the set of characteristic times which are logarithmically distributed from 10 ps to a 10 μs with 50 points per decade $\tau_i = 10^{-2+i/50}$ns, $i = 0...350$.

The distribution of amplitudes A_i is a solution of weighted mean square fitting problem for a set of counts d_k at times t_k and requires the minimization of

$$S(p) = \sum_k \frac{(d_k - f(t_k))^2}{d_k + 1} + p\sum_i A_i^2 \qquad (2)$$

The denominator accounts for Poisson statistic of counts d_k. The analysis needs therefore to use some regularizations. We used Tikhonov regularization (the last term in Eq.(2)) which results in distribution of amplitudes without significant oscillations. The problem is constrained minimization since all amplitudes are supposed to be positive. Parameter p is chosen in a way that $S(p) < 1.01S(0)$ (i.e. this term do not increase the error in residuals) but provide relatively smooth distribution of the amplitudes. The data, fitted curves and normailzed residuals obtained considering the convolution with the impulse response function are presented in figure 6.

4 Long time decay analysis

As described in the main paper, the slow component of the C/C 4ML NPLs sample can be described as an hyperbolic power-law distributions. For illustration, the fluorescence decay-time measurement has been fitted by a t^{-n} law, and for tome larger than 4 ns, we obtained $n = 1.07$ as the best values (Figure 7).

5 Pseudo-Voigt fitting

As shown in 8 for the C/C 4ML sample, the emission spectra cannot be fitted neither by a Gaussian shape (dashed blue) nor a Lorentzian shape (dashed green) function. We have then used a pseudo Voigt profile corresponding to a linear combination of a Gaussian function and a Lorentzian function centered on the same value (solid black).

6 Pseudo-Voigt fitting

As plotted in figure 9 for the C/C 4ML sample, the emission spectra obtained under various intensities of excitation have been fitted with a pseuso-Voigt profiles. For the lowest intensity (2.7 W cm^{-2}), a single pseudo-Voigt function is enough while for higher intensities, 2 pseudo-Voigt functions are required allowing to obtain the X_0 and XX emission energies.

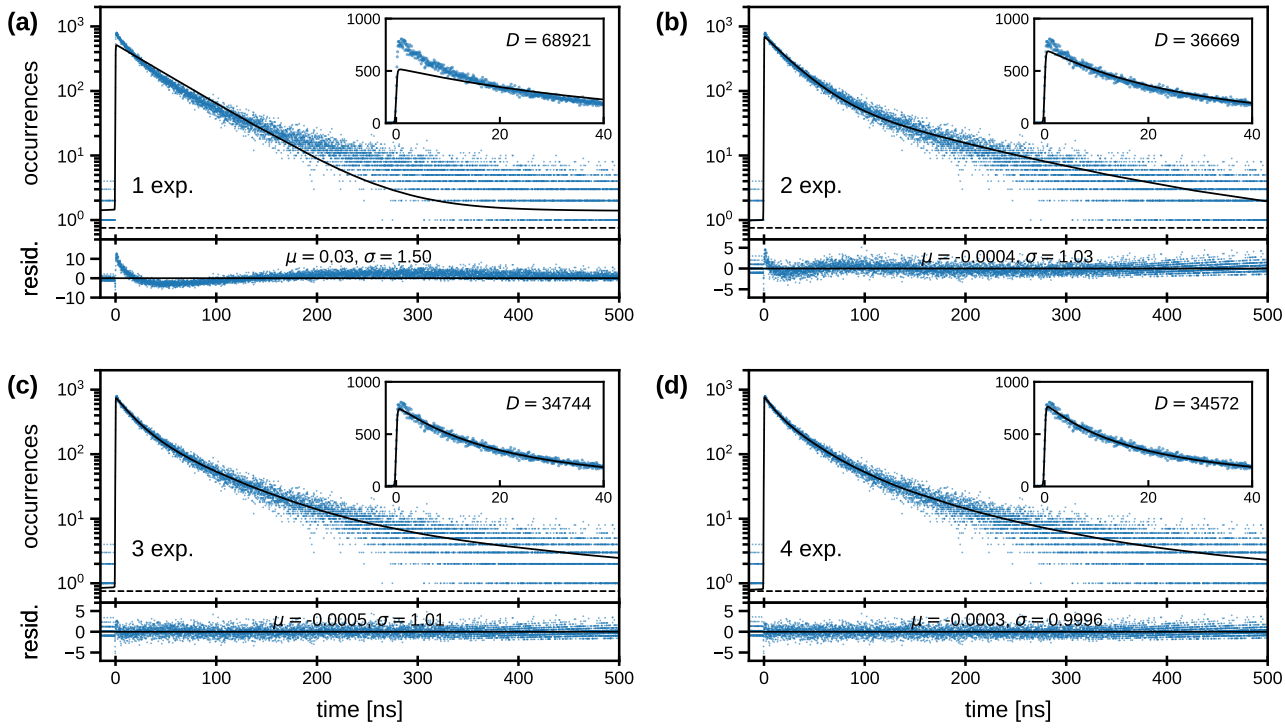

Figure 2 Photoluminescence decay curve of 4 nm core/shell nanoplatelets (filled circles, same data as in Fig. 2 c) with maximum-likelihood adjustments of a model with **(a)** one, **(b)** two, **(c)** three, and **(d)** four exponential decay components (solid lines); dashed lines indicate the average background level before the laser pulse ($t < 0$). The bottom panels show the normalized residuals of each fit. The average value μ and the standard deviation σ of the residuals, as well as the Poisson deviances D, were calculated over the full range of the measured decay curve (2 µs).

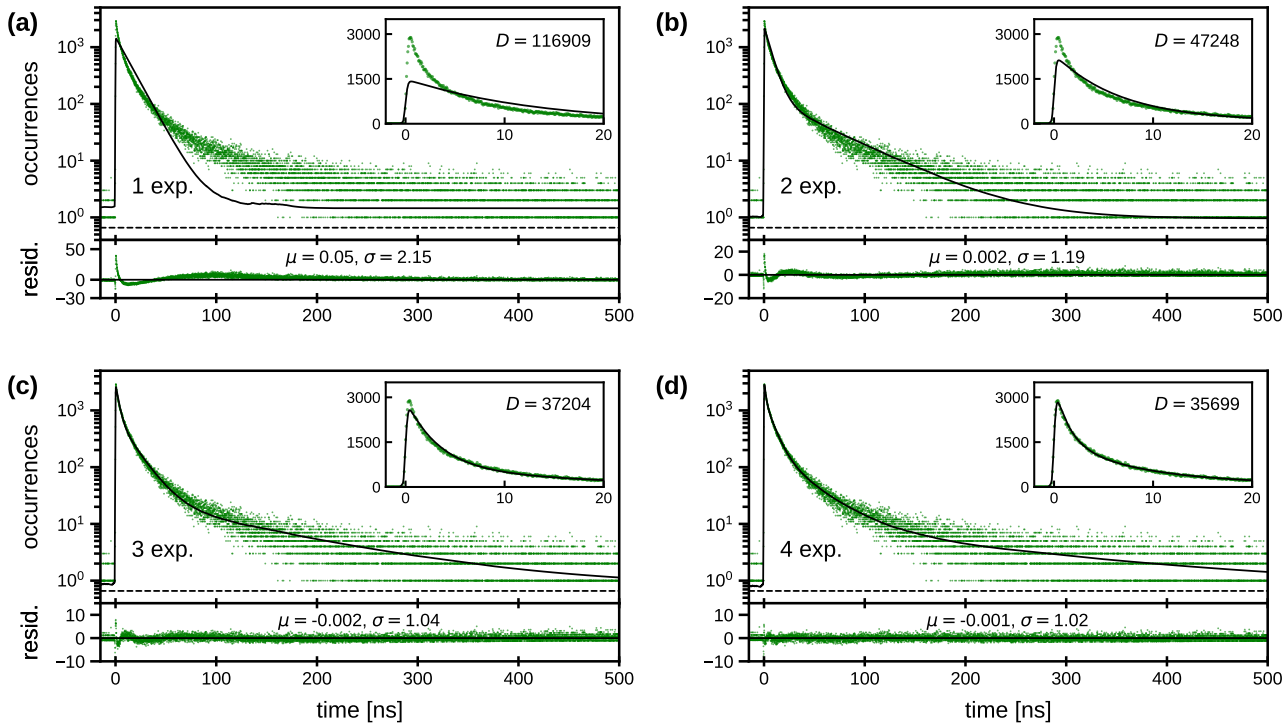

Figure 3 Photoluminescence decay curve of 3 nm core/shell nanoplatelets (filled circles, same data as in Fig. 2 c) with maximum-likelihood adjustments of a model with **(a)** one, **(b)** two, **(c)** three, and **(d)** four exponential decay components (solid lines); dashed lines indicate the average background level before the laser pulse ($t < 0$). The bottom panels show the normalized residuals of each fit. The average value μ and the standard deviation σ of the residuals, as well as the Poisson deviances D, were calculated over the full range of the measured decay curve (2 µs).

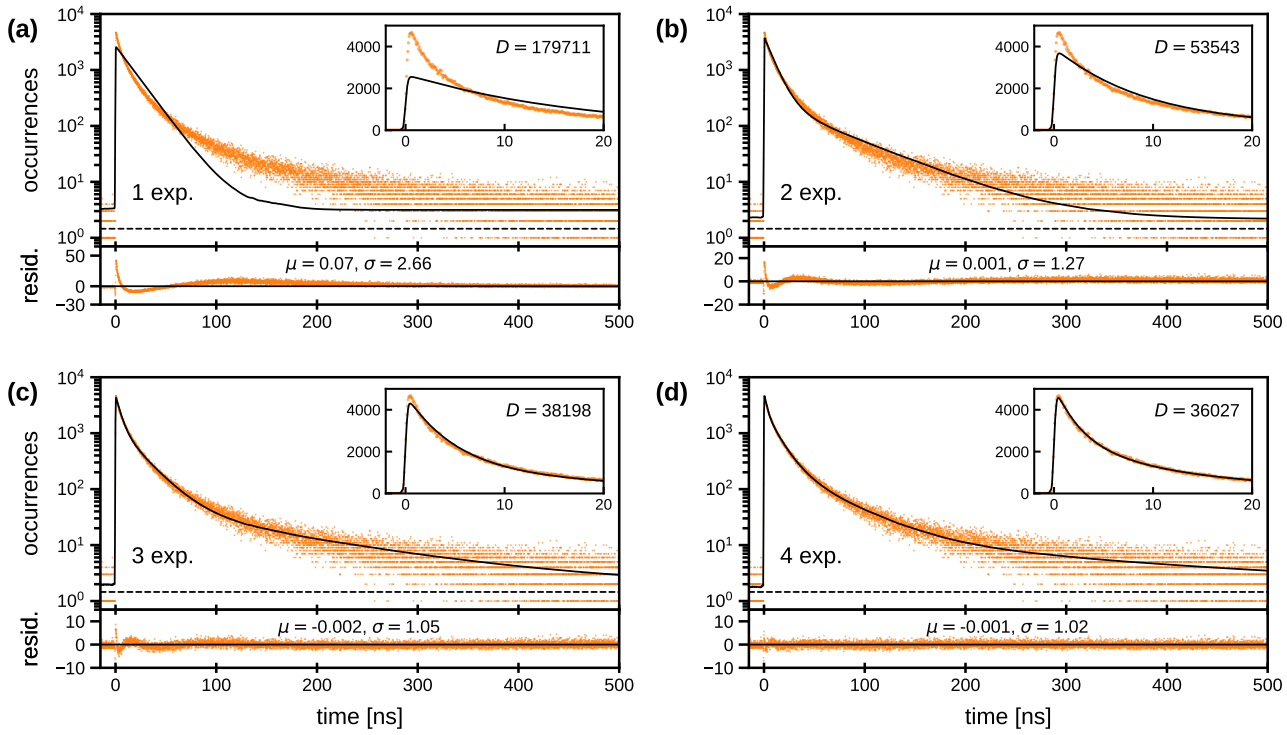

Figure 4 Photoluminescence decay curve of 2 nm core/shell nanoplatelets (filled circles, same data as in Fig. 2 c) with maximum-likelihood adjustments of a model with **(a)** one, **(b)** two, **(c)** three, and **(d)** four exponential decay components (solid lines); dashed lines indicate the average background level before the laser pulse ($t < 0$). The bottom panels show the normalized residuals of each fit. The average value μ and the standard deviation σ of the residuals, as well as the Poisson deviances D, were calculated over the full range of the measured decay curve (2 µs).

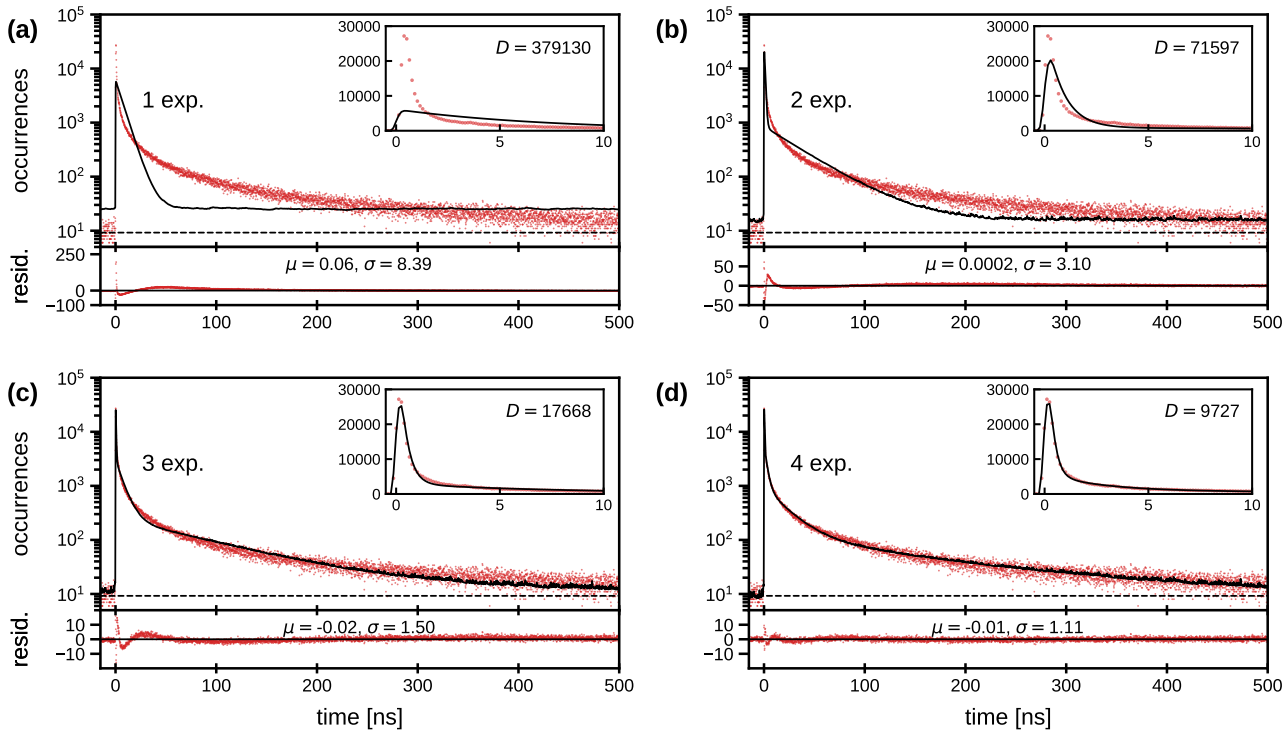

Figure 5 Photoluminescence decay curve of 4 ML core/crown nanoplatelets (filled circles, same data as in Fig. 2 c) with maximum-likelihood adjustments of a model with **(a)** one, **(b)** two, **(c)** three, and **(d)** four exponential decay components (solid lines); dashed lines indicate the average background level before the laser pulse ($t < 0$). The bottom panels show the normalized residuals of each fit. The average value μ and the standard deviation σ of the residuals, as well as the Poisson deviances D, were calculated over the full range of the measured decay curve (1 µs).

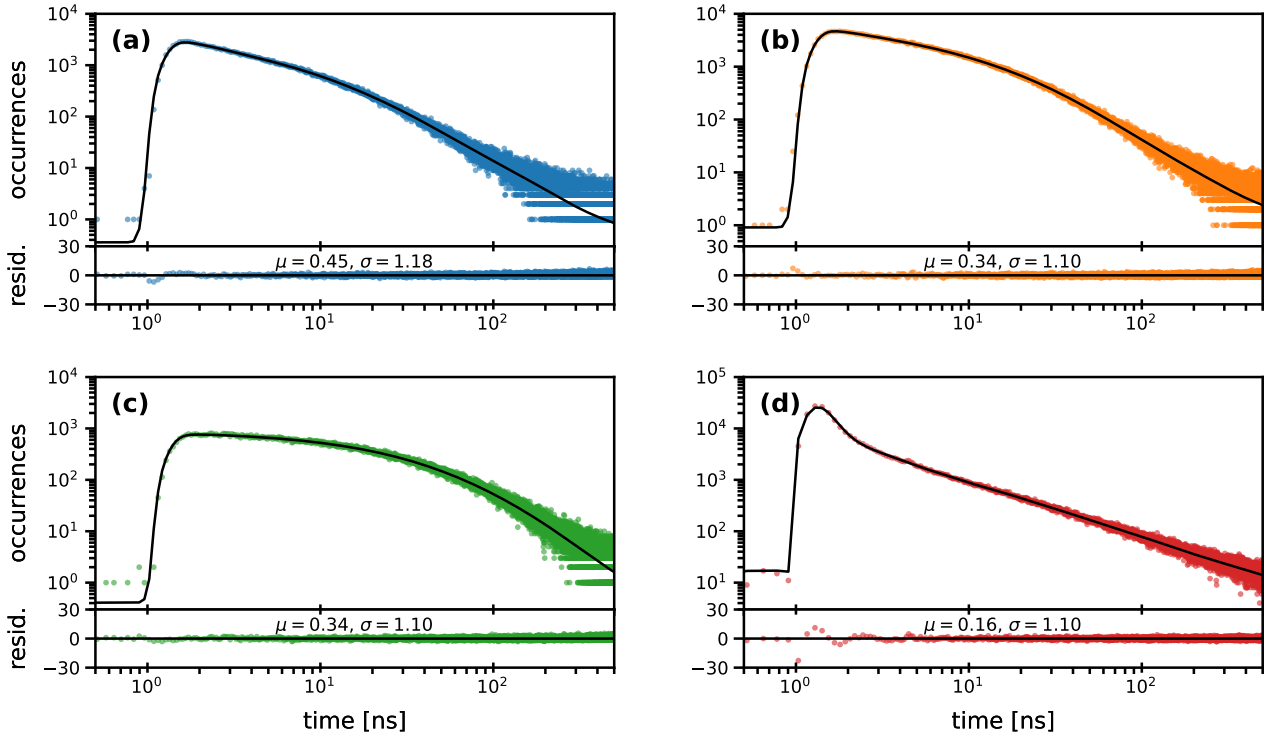

Figure 6 Photoluminescence decay curves of 4 NPLS samples (filled circles, same data as in Fig. 2 c) with log-distributed decay time component adjustments for thicknesses **(a)** 4 nm, **(b)** 3 nm, **(c)** 2 nm, and **(d)** 4ML. (solid lines); The bottom panels show the normalized residuals of each fit. The average value μ and the standard deviation σ of the residuals, were calculated over the full range of the measured decay curve (1 µs).

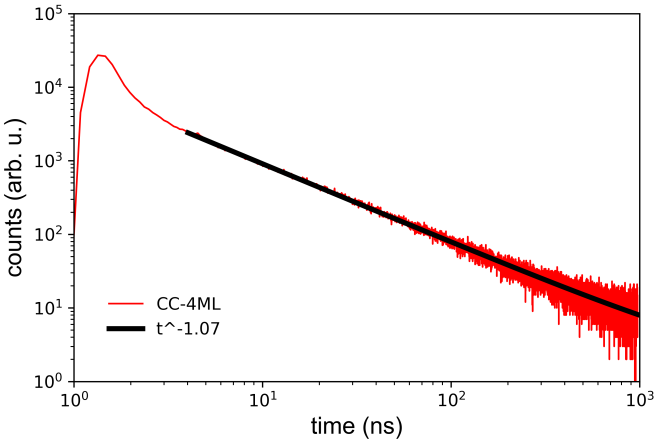

Figure 7 Fluorescence decay time measurement and its hyperbolic fitting for t>4ns

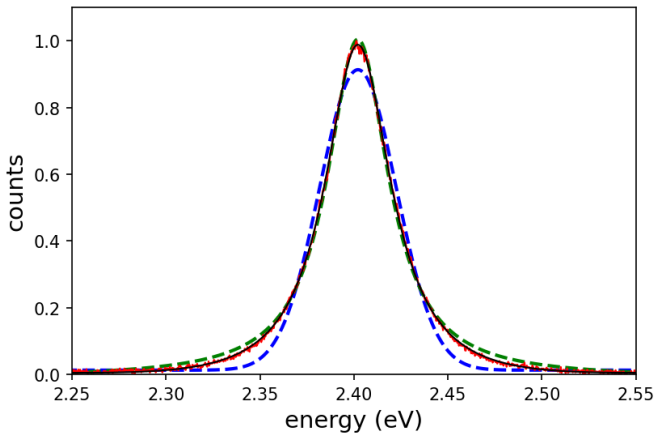

Figure 8 Red- Experimental emission spectrum of the C/C-4ML sample (I=2.7 W cm^{-2}). Dashed blue curve corresponds to the best fitting of the emission spectrum using a Gaussian function, dashed green with a Lorentzian function and solid black with a pseudo-Voigt profile

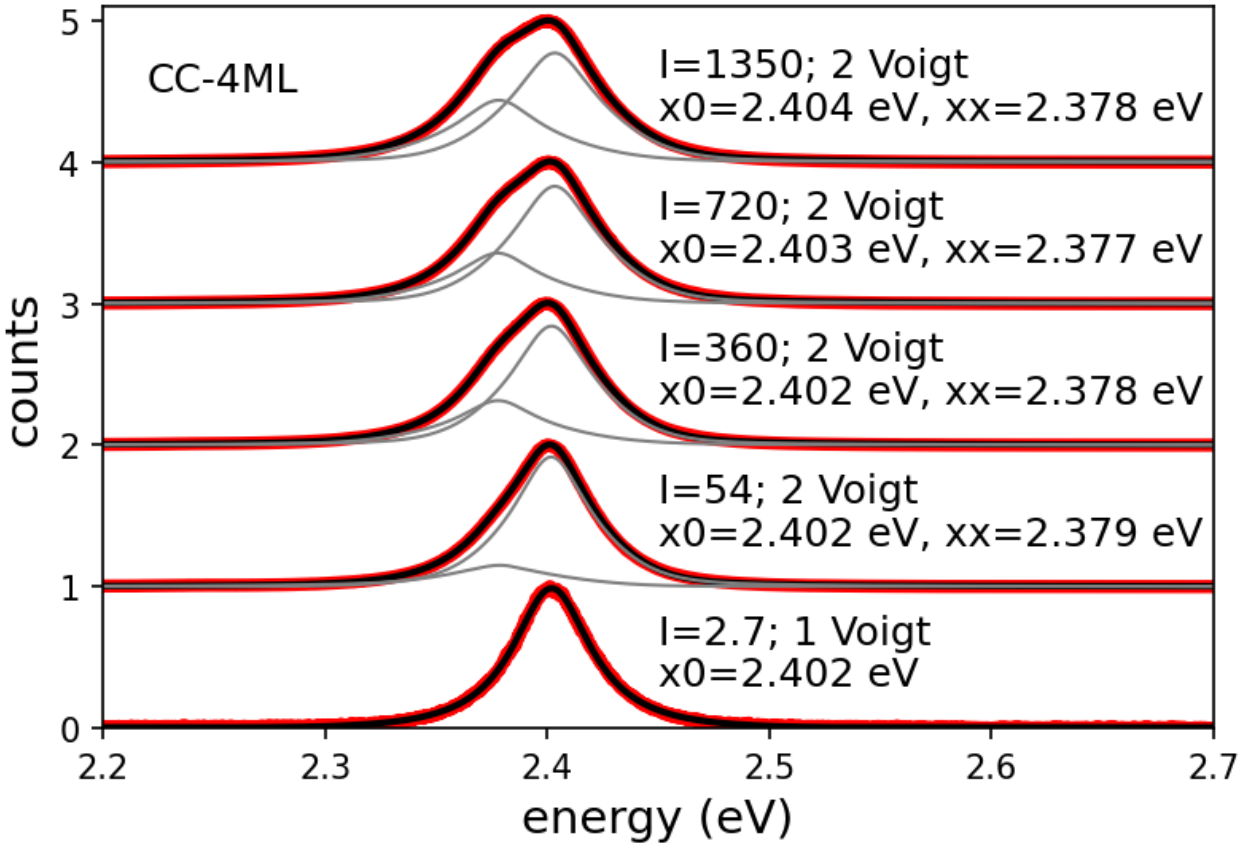

Figure 9 Solid Red: experimental emissions obtained at different intensities of excitation (I) expressed in W cm^{-2}. The thick black curve corresponds to the best fit obtained and the thin solid grey lines are the 2 pseudo-Voigt functions composing the whole fitted function (solid thick black).